Experimental study of the $6^1\Sigma_g^+$ state of the rubidium dimer

Phillip T. Arndt,[1] Vladimir B. Sovkov,[2,3] Jie Ma,[3,4] Xinhua Pan,[1] David S. Beecher,[1] Jeng Y. Tsai,[1] Yafei Guan,[1] A. Marjatta Lyyra,[1] and Ergin H. Ahmed[1,*]

[1]*Physics Department, Temple University, Philadelphia, Pennsylvania 19122-6082, USA*

[2]*St. Petersburg State University, 7/9 Universitetskaya nab., St. Petersburg 199034, Russia*

[3]*State Key Laboratory of Quantum Optics and Quantum Optics Devices, Institute of Laser Spectroscopy, College of Physics and Electronics, Shanxi University, Taiyuan 030006, China*

[4]*Collaborative Innovation Center of Extreme Optics, Shanxi University, Taiyuan, Shanxi 030006, People's Republic of China*

(Received 11 January 2019; revised manuscript received 18 April 2019; published 22 May 2019)

This paper reports a high-resolution experimental study and a numerical analysis of the Rb_2 $6^1\Sigma_g^+$ ion-pair state. A large number of rovibrational term values spanning a wide range of the rotational and vibrational quantum numbers were measured using the optical-optical double-resonance technique. The set of term values was simulated with a model of a piecewise multiparameter potential-energy function based on the generalized splines. This function reproduces the experimental data with reasonable accuracy and, in addition, allows us to incorporate in the potential function the nontrivial features at longer internuclear range, such as multiple wells, predicted by the *ab initio* calculations.

DOI: 10.1103/PhysRevA.99.052511

I. INTRODUCTION

The alkali-metal molecules are of broad interest in a number of areas of research, including ultracold ground-state molecules, atom-molecule collisions, molecular Bose-Einstein and Fermi gases, and optimal control of chemical reactions [1–8]. The rubidium dimer, in particular, is widely used for these purposes due to the convenient transitions for laser cooling of the rubidium atoms from which the molecules are formed by photoassociation or magnetoassociation. In all of these applications, the energy-level structure of the molecules is of critical importance. A number of *ab initio* studies of the Rb_2 electronic structure exist [9–19] and, even though the accuracy of such calculations has improved significantly, they are not yet a substitute for precise experimental measurements. In experiments, such as the one reported here, an absolute accuracy of the order of $0.02\,cm^{-1}$ is easily achieved. This is at least one to two orders of magnitude better than the accuracy of the best excited-state Rb_2 dimer *ab initio* calculations [18,19] to date.

The low-lying electronic states of Rb_2, such as the singlet $X^1\Sigma_g^+$ [20–22] and triplet $a^3\Sigma_g^+$ [23] ground states, and the $A^1\Sigma_u^+ \sim b^3\Pi_u$ [24,25] intermediate states as well as some other excited upper states have been studied experimentally [21,26–65], but the higher-lying ion-pair states such as the $6^1\Sigma_g^+$ state have not been observed experimentally. Highly excited $^1\Sigma$ states of alkali-metal molecules are typically significantly perturbed and exhibit shelf regions and secondary wells due to couplings with other states as well as the ion-pair $M^+ - M^-$ Coulomb potential (M denotes the alkali-metal atom) [66]. This gives rise to unusual properties, including extremely long-range vibrations, large dipole moments, and a near-infinite manifold of vibrational states. They are attractive for the detection of ultracold molecules using the resonantly enhanced multiphoton ionization (REMPI) technique [67–73] in a broad internuclear range. They can also be used for Raman transfer of the molecular population from large internuclear distance to the covalent bonding region. In addition, as suggested in Ref. [74], such Rydberg states could be used to create ultracold-atomic negative ions to determine the atomic electron affinity or to create long-lived wave packets. Ion-pair states of other diatomic molecules have been studied experimentally including the XUV + UV excitation scheme in H_2 [75], dissociation dynamics of long-lived ion-pair states of Cl_2 [76], and determination of the deuterium electron affinity from measurements of the ion-pair dissociation energies of the HD molecule [77].

We report here an experimental observation of the $6^1\Sigma_g^+$ state of the rubidium dimer. The experiment was done using the optical-optical double-resonance (OODR) technique. The observed vibrational progression in the experiment was identified as belonging to the $6^1\Sigma_g^+$ state using *ab initio* predictions [18,19]. In addition, at lower energies, two other vibrational progressions were observed, which we are currently in the process of identifying. The $6^1\Sigma_g^+$ state results were analyzed in combination with the *ab initio* data for this state from Refs. [18,19] with a model of a piecewise multiparameter potential-energy function [25,78–82] based on the generalized splines. This allowed us to incorporate in our potential-energy functions the nontrivial features predicted by the *ab initio* calculations.

II. EXPERIMENT

The experimental details have been described previously in Ref. [83]. Briefly, the Rb_2 molecules were generated in a heat-pipe oven loaded with rubidium metal containing ^{85}Rb

*erahmed@temple.edu

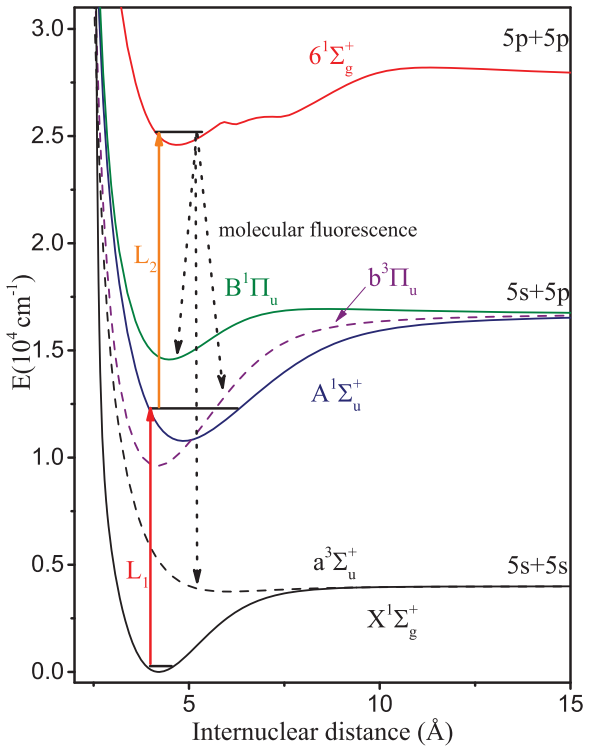

FIG. 1. Excitation scheme and potential-energy curves of the Rb_2 dimer. The potential curves are *ab initio* calculations from Ref. [19]. Solid vertical lines represent the laser excitations, while the dashed downward lines depict the possible fluorescence decay channels.

and ^{87}Rb isotopes in the natural abundance ratio. In the experiment, only $^{85}Rb_2$ isotopomer transitions were selectively probed. The temperature at the center of the oven was maintained at 180 °C using electrical heaters. Argon at 2 Torr pressure (measured at room temperature) was used as a buffer gas. To reach the levels of the $6^1\Sigma_g^+$ state, a cascade double-resonance excitation scheme with an intermediate level from the $A^1\Sigma_u^+ \sim b^3\Pi_u$ manifold [25], arising from the strong spin-orbit coupling of the $A^1\Sigma_u^+$ and $b^3\Pi_u$ states, was used in the experiment (see Fig. 1). In the experiment, single-mode tunable ring lasers, Coherent 899-29 Ti:sapphire (L_1) and 699-29 with LDS722 dye (L_2), were used in the counterpropagating configuration. The L_1 laser excited the molecules from thermally populated rovibrational levels of the $X^1\Sigma_g^+$ ground state to an intermediate level from the $A^1\Sigma_u^+ - b^3\Pi_u$ manifold (see Table I).

To identify and confirm the assignment of each intermediate level used, fluorescence spectra to the ground state were recorded with an FTIR spectrometer (BOMEM DA8) for the P and R excitation branches. An example of such fluorescence spectra is given in Fig. 2. The energy of the intermediate level was obtained from the energy of the initial $X^1\Sigma_g^+$ levels, calculated from the Dunham constants published in Ref. [22] and the laser transition frequencies for the P and R excitation branches, which were measured and calibrated with the FTIR spectrometer. The FTIR spectrometer itself was calibrated with a uranium hollow cathode atlas [84]. The resonances of the probe laser, tuned in the range 13 300−14 000 cm^{-1}, to

TABLE I. List of levels belonging to the $A^1\Sigma_u^+ - b^3\Pi_u$ manifold used as intermediates in the OODR excitation scheme [25].

n'	J'	E' (cm^{-1})	n'	J'	E' (cm^{-1})
80	1	11031.6644	83	1	11080.9060
93	1	11205.3185	107	1	11379.3966
117	1	11379.3966	74	10	10964.1468
80	10	11033.5989	83	10	11082.7631
93	10	11207.1703	107	10	11381.2240
117	10	11508.2995	131	10	11674.3385
144	10	11840.6749	148	10	11885.6737
158	10	12004.9390	76	30	11006.3037
79	30	11048.4095	83	30	11096.9272
97	30	11271.6052	107	30	11395.1452
117	30	11522.5347	127	30	11644.6055
78	70	11111.7100	82	70	11163.2669
106	70	11462.9966	119	70	11631.7487
129	70	11753.9396			

the $6^1\Sigma_g^+$ state were observed by detecting fluorescence to the $a^3\Sigma_u^+$ state in the 500 nm range (4303 and 4305 Kopp Glass filters) with a photomultiplier tube (R928P Hamamatsu Photonics) mounted on one of the side arms of the heat pipe. Despite the forbidden nature of the fluorescence transition, we have observed strong signals due to the significant spin-orbit coupling of the $6^1\Sigma_g^+$ state with nearby triplet states. The photomultiplier tube current was amplified with a lock-in amplifier (SRS 850 Stanford Research) and recorded as a function of the frequency of the probe laser, while the pump laser was modulated at a rate of about 1 kHz. This ensures that only double-resonance signals are recorded in the spectra. An example of such excitation spectra is given in Fig. 3. In addition to the expected P and R main branches, we observed a number of satellite lines due to collisions with the argon and rubidium atoms present in the heat pipe. These lines allowed us to gather additional rotational data for each observed vibrational level. Part of the observed collisional lines was solely used to determine the energies of the intermediate levels from which they originate. For example, to determine the energy of the $J' = 28$ intermediate level, $E(J' = 28)$, we subtracted the energy difference between the $R(28)$ and $P(30)$ lines from the term value of the $J' = 30$ main-line intermediate level $[E(J' - 2) = E(J') + P(J') - R(J' - 2)]$ already determined by the pump laser. Then, from the energy of the $J' = 28$ level and the transition frequency of the $P(28)$ collisional line, the energy of the upper state with rotational quantum number $J = 27$ was determined. In the next step, the energies of the $J' = 26$ intermediate and $J = 25$ upper states were determined. This cascade process was continued downward until all observed corresponding satellite lines were used. Similarly, for satellite lines originating from intermediate levels with J' greater than the main-line intermediate, we used the expression $E(J' + 2) = E(J') + R(J') - P(J' + 2)$ to propagate upward the intermediate-level energies, which allowed us to obtain term values of upper state levels with rotational quantum number $J = (J' + 1) + 2, (J' + 1) + 4, \ldots$, and so on. The experimental data is illustrated in Fig. 4 and the details of the observed transitions are given in the Supplemental Material [85].

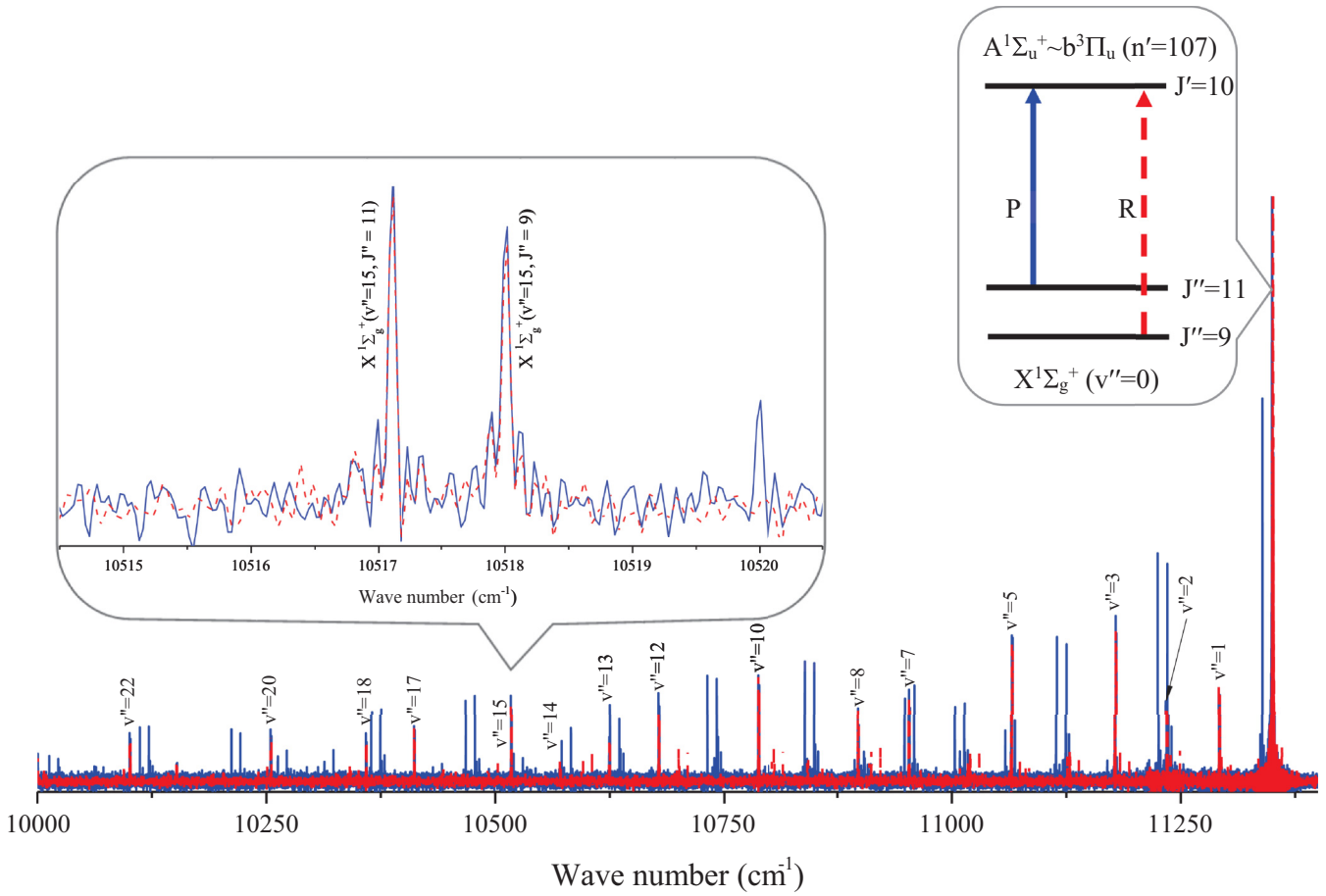

FIG. 2. Resolved fluorescence spectra used to confirm the $A^1\Sigma_u^+ - b^3\Pi_u$ ($n' = 107, J' = 10$) intermediate level. The confirmation process involves identifying peaks forming a vibrational progression of P and R lines that occur in both spectra and using the $X^1\Sigma_g^+$ state term values [22], assigning them to specific transitions from the target upper level, in this case $A^1\Sigma_u^+ - b^3\Pi_u$ ($n' = 107, J' = 10$), to rovibrational levels of the $X^1\Sigma_g^+$ state.

The rotational assignment of the term values is based on the excitation scheme, while the vibrational assignment is based on the predictions of the *ab initio* potential functions [18,19].

III. ANALYSIS

The model multiparameter potential-energy function employed here was presented in our earlier article [86]. However, we only mentioned an attempt (generally speaking, successful) to use it in the analysis of the ground singlet and triplet states of the cesium dimer, while the final results were presented in a form of the MLR3 (Morse Long Range 3) function by Coxon and Hajigeorgiou [80]. Later [83], we applied this approach to a combination of experimental and *ab initio* data on the Rb_2 $3^1\Pi_g$ state. It allowed us to adequately reproduce the observed rovibrational term values and to approximate the *ab initio* potential-energy function with a uniform accuracy in its entire range, including some nontrivial bends. The *ab initio* potential [19] of the Rb_2 $6^1\Sigma_g^+$ state predicts more complicated features such as multiple wells, which do not occur for the Rb_2 $3^1\Pi_g$ state. One of the purposes of the present article was to check the ability of our model potential to reproduce those features adequately.

Below we give this model function in a somewhat simplified modification in order to avoid details not being employed in the actual computations. More general equations can be found in Refs. [83,86]. Our model potential function has the same form as the one employed in a number of earlier works (see Refs. [25,72,81,82], and references therein):

$$U_{pw}(R) = U_\infty + \begin{cases} u_0 + u_1/R^{N_s}, & R \leqslant R_s \\ U_{\mathrm{pwm}}(y_{p,a}(R, R_m)), & R_s < R < R_l \\ -\sum_k \left(C_{n_k}/R^{n_k}\right), & R \geqslant R_l, \end{cases} \quad (1)$$

where all three pieces are smoothly joined in the sense of $\mathbb{C}^n$, with $n = 1$ in our case ($\mathbb{C}^n$ is the space of functions, whose derivatives up to the nth order are continuous), R is the nuclear separation, and the long-range term describes the prevailing multipole-dispersion forces [87–89] with U_∞ being the energy at the dissociation limit and C_{n_k} being the dispersion coefficients. Traditionally [25,72,81,82], the middle part of Eq. (1) is described by a polynomial of an argument

$$y_{p,a}(R, R_m) = \frac{R - R_m}{R + aR_m}. \quad (2)$$

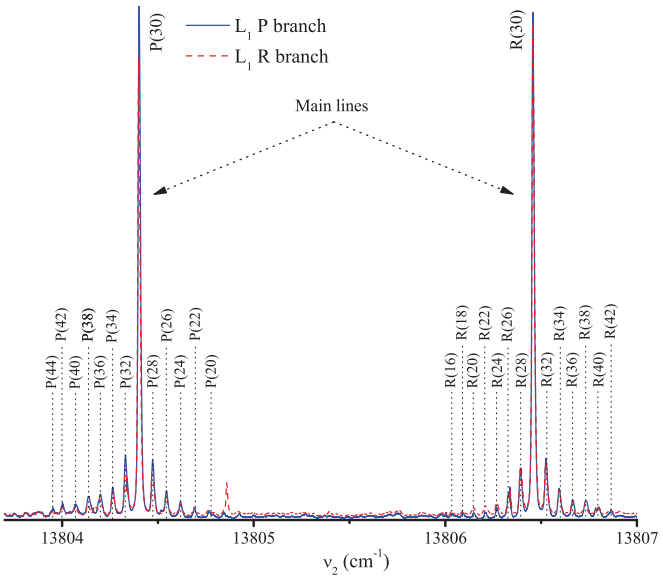

FIG. 3. Excitation spectrum of the $6^1\Sigma_g^+(v=13)$ vibrational level from the $A^1\Sigma_u^+ - b^3\Pi_u$ ($n'=97, J'=30$) intermediate level. A number of collisional satellite lines are observed arising from collisional transfer of the population in the intermediate state to neighboring rotational levels. In the figure, only the collisional lines with independently confirmed assignment are labeled. In homonuclear molecules, the propensity rule for inelastic collision-induced rotational transitions determines that only even-J changing collisional lines are observed ($\Delta J = \pm 2, 4, 6, \ldots$).

Our version differs from the traditional one in two points. First, in place of Eq. (2) we use the following generalization:

$$y_{p,a}(R, R_m) = \frac{R^p - R_m^p}{R^p + aR_m^p}, \tag{3}$$

where p (as a rule, integer positive) is the Šurkus parameter [90], which has proved to be very useful for the generalized

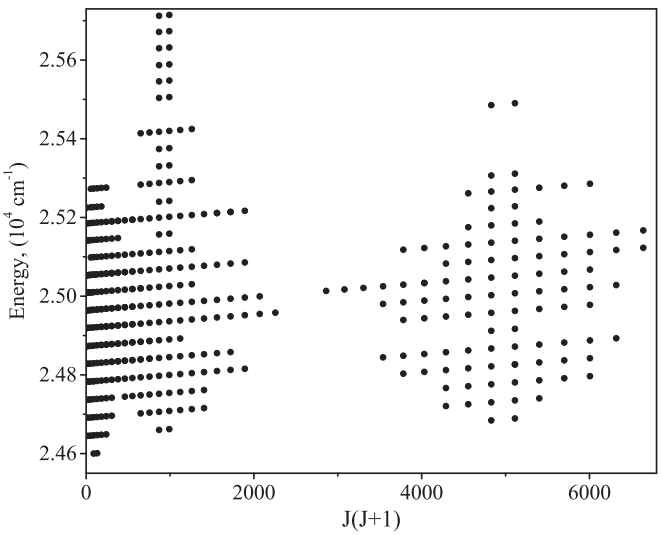

FIG. 4. Experimentally observed 787 rovibrational levels spanning the range of the rotational quantum number $J = 0$ through 83 and the vibrational quantum number $v = 0$ through 25 (about 1/4 of the potential well depth).

Morse functions [78–81]. Second, in place of the polynomial, we use a generalized spline function, similar to the one applied to the dependencies of the quantities G_v and B_v on v in our work [64] (see also Ref. [91]):

$$U_{pwm}(x) = \sum_{n=1}^{n_b} b_n x^{l_n^{(b)}} + \sum_{k=1}^{m_a} \sum_{n=1}^{n_a} \left[a_n^{(k)} \theta\left(x - x_a^{(k)}\right) + \tilde{a}_n^{(k)} \theta\left(x_a^{(k)} - x\right) \right] \left(x - x_a^{(k)}\right)^{l_n^{(a)}}, \tag{4}$$

with

$$\theta(x) = \begin{cases} 1 & (x \geqslant 0) \\ 0 & (x < 0), \end{cases}$$

for which the polynomial is just a partial case ($a_n^{(k)} = 0, \tilde{a}_n^{(k)} = 0$). This function experiences discontinuities of the derivatives of orders $l_n^{(a)}$ at knots $x_a^{(k)}$. Notice that a formally equivalent function is the one with either $a_n^{(k)} = 0$ or $\tilde{a}_n^{(k)} = 0$. However, keeping both terms makes the function more flexible and capable of easily correcting its behavior at the right or left branch, while not influencing the opposite one. The variable x is computed with Eq. (3) from the current nuclear separation R, and the parameters $x_a^{(k)}$—the same way from the anchor points $R_a^{(k)}$. All the notations in the above equations that are not disclosed explicitly represent formal parameters of the model.

The set of data to be fitted to this model included the experimental term values of the present work (see the Supplemental Material [85]) and the *ab initio* potential functions [19]. The weights of the *ab initio* data were rather relaxed, but we regulated them in the course of the computations in order to get an

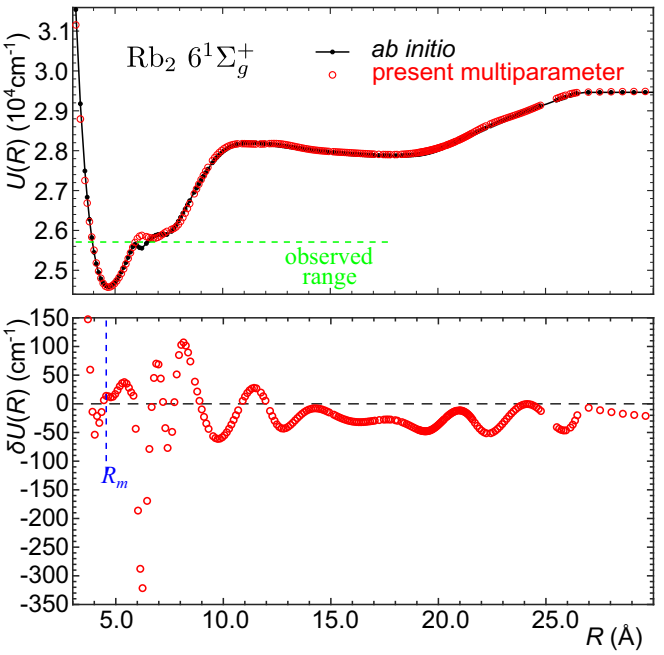

FIG. 5. Upper panel: potential-energy functions of the Rb_2 $6^1\Sigma_g^+$ state, *ab initio* [18,19] (solid line) and present (circles). Lower panel: difference between the *ab initio* [18,19] and present potential-energy functions. The range of the observed rovibrational term values and the position R_m of the potential minimum are also shown.

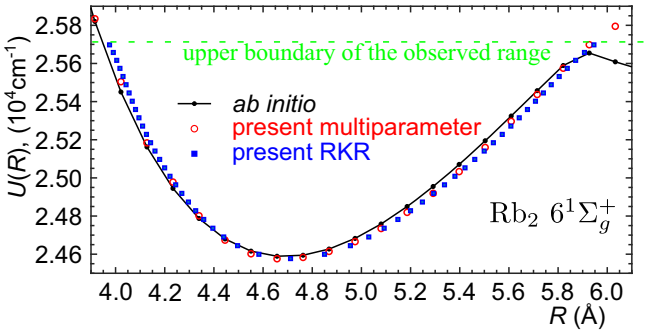

FIG. 6. Potential-energy functions of the Rb_2 $6^1\Sigma_g^+$ state: *ab initio* [18,19] (solid line), present model (circles), and present RKR (squares).

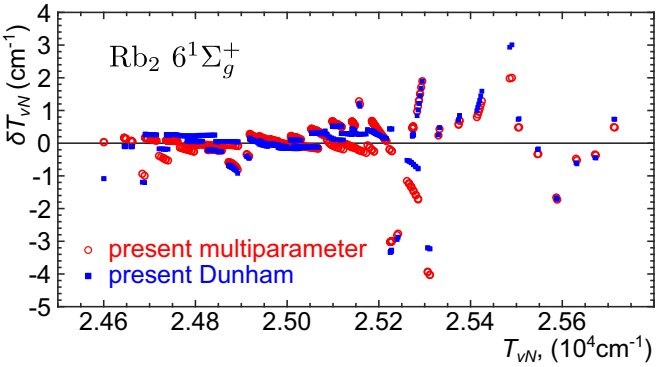

FIG. 7. Residuals of the experimental rovibrational term values of the Rb_2 $6^1\Sigma_g^+$ state reproduced with the potential-energy function of the present work (open circles) and with the straightforward Dunham series (solid squares).

approximately uniform accuracy in the reproduction of the experimentally observed as well as unobserved ranges. The term values were computed with the familiar Numerov method [92–94]. The fitting itself was done with the help of our computational package OPTIMIZER described elsewhere [94], which realizes the nonlinear least-squares fitting based on the Levenberg-Marquardt algorithm [95] using the singular-value decomposition (SVD) [96] of the design matrix.

The resulting model function is compared to the *ab initio* counterpart in Figs. 5 and 6 (trivial long-range and short-range asymptotes are not shown in order to better illustrate the more important middle parts). Figure 6 also shows the straightforwardly constructed Rydberg-Klein-Rees (RKR) [97–100] potential. The model multiparameter function and the RKR potential are also tabulated in the Supplemental Material [85].

The final sets of the parameters of the model functions are listed in Table II . These parameters were subjected to the sequential rounding-off procedure similar to the one described in Ref. [101], and they adequately reproduce the spectroscopic information. The Dunham coefficients, which were determined from the experimental term values directly and were used to construct the RKR potentials, are tabulated in Table III.

The residuals of the experimental term-values simulation with our final potential-energy functions are shown in Fig. 7. We note that the term values with obvious strong perturbations were downweighted in the course of the computations for a better robustness of the overall procedure.

IV. DISCUSSION

Figure 7 show that the experimental term values are clearly perturbed. There is nothing surprising about this for highly excited electronic and rovibronic states due to their density in terms of energy and the various allowed nonadiabatic couplings. The perturbations are drastically enlarged in the region around 25 300 cm^{-1}, indicating resonances of energy levels. This is the same region where the biggest perturbations were observed for the $3^1\Pi_g$ state [83]. This fact indicates that these electronic states are coupled with each other and, maybe, with other states in this energy region. A detailed analysis of the perturbations can only be done via a complex model including all the interactions, which is outside the scope of the present article.

Some of the observed levels of the $6^1\Sigma_g^+$ state lie a little higher than the barrier predicted by the *ab initio* calculations (Fig. 6). However, they retain a rather regular pattern, indicating that this barrier, if it exists, is not actually reached yet. This is why in this region the deviation of our semiempirical

TABLE II. Parameters of the model function given by Eqs. (1) and (4) constructed for the Rb_2 $6^1\Sigma_g^+$ state in the present work. All the values are measured in cm^{-1} and Å.

Param.	Value	Param.	Value	Param.	Value	Param.	Value
p	2	N_s	5.8	n_1	3	n_2	6
U_∞	29468	$R_m = R_e$	4.6828	a	0.3185		
u_0	−5874.0975	u_1	6.1479×10^6	C_3	-1.7576815×10^6	C_6	3.407902×10^{10}
R_s	4	R_l	26.7	$R_a^{(1)}$	4.28	$R_a^{(2)}$	6.32
$R_a^{(3)}$	7.68	$R_a^{(4)}$	12.32	$R_a^{(5)}$	21.5	$b_0 = -D_e$	−4892.88
b_2	12792	b_3	−23000	b_4	92300	b_5	277200
b_6	-3.03×10^6	b_7	5.776×10^6	b_8	2.038×10^7	b_9	-6.566×10^7
b_{10}	-6.43×10^7	b_{11}	1.889635×10^8	b_{12}	9.5×10^7	b_{13}	-5×10^7
b_{14}	-5.065×10^7	$\tilde{a}_5^{(1)}$	-6.46×10^7	$\tilde{a}_6^{(1)}$	-3.9×10^8	$a_4^{(2)}$	-2.72×10^7
$a_5^{(2)}$	6×10^7	$a_6^{(2)}$	-9.78×10^8	$a_4^{(3)}$	-9.7×10^7	$a_6^{(3)}$	-3.095×10^9
$a_4^{(4)}$	3.5×10^8	$a_5^{(4)}$	-2×10^9	$a_6^{(4)}$	2.23×10^{10}	$a_3^{(5)}$	-6.7×10^8
$a_4^{(5)}$	5×10^{10}	$a_5^{(5)}$	-1.16×10^{12}				

TABLE III. Dunham coefficients Y_{ij} of the Rb_2 $6^1\Sigma_g^+$ state (cm^{-1}).

$i\backslash j$	0	1	2
0	$T_e + Y_{00} = 24577.07(0.27)$	$1.7885(0.0027) \times 10^{-2}$	-1.15745×10^{-8}
1	44.471(0.179)	$-6.35(0.31) \times 10^{-5}$	
2	0.46782(0.04115)		
3	−0.061607(0.004140)	$Y_{00} = 0.144$	
4	$2.8216(0.1864) \times 10^{-3}$	$R_e = 4.7117$ Å	
5	$-4.537(0.305) \times 10^{-5}$		

potential from the *ab initio* one is the biggest. The RKR potential, which was computed independently, exhibits behavior similar to our model potential in the region of the barrier, i.e., it confirms this observation. Nevertheless, we tried to construct a model, which reproduced the *ab initio* potential with an appropriate accuracy in the regions not observed in the experiment as well, in order to demonstrate the capability of this multiparameter function to deal with the potentials containing nontrivial bends and multiple wells.

The only purpose of the short-range and long-range parameters in Table II is an adequate and smooth approximation of the *ab initio* potentials [18,19]; they do not provide any other empirical or theoretical information. We do not claim here that our potential-energy function physically correctly describes the near-dissociation properties of the state.

Starting from the molecular electronic ground state, our results are limited to relatively short internuclear distances. This is due to poor Franck-Condon factors to levels of the ion-pair states that extend or are confined (secondary well) to the long range. These levels can be accessed starting from the atomic limit. For example, using the atomic limit and the Rb second resonance doublet transition, Rb_2 ion-pair satellite bands have been reported at large internuclear distance in absorption measurements in a hot dense Rb vapor [102]. In addition, the authors propose that by using single-photon photoassociation, these long-range ion-pair states can be used to produce ultracold Rb_2 molecules in the ground state. Another approach to reach these long-range ion-pair molecular levels involves using ultracold atoms and Feshbach resonances [74,103].

V. CONCLUSIONS

We have observed a large set of rovibrational levels of the Rb_2 $6^1\Sigma_g^+$ ion-pair state. To analyze the experimental results and to generate a potential curve, a model multiparameter potential-energy function based on the generalized splines was constructed. This approach allowed us to simulate the experimental term values with an adequate quality and to approximate the available *ab initio* potential function [19] in its entire range with the appropriate accuracy.

ACKNOWLEDGMENTS

This work was supported by the National Science Foundation Grant No. NSF PHY 1607432, the Lagerqvist Research Fund of Temple University, the collaborative grant of the Russian Foundation for Basic Research (RFBR) and NNSF of China (Grant No. 18-53-53030 in the RFBR classification), the National Key R&D program of China (Grant No. 2017YFA0304203), and the NNSFC (Grant No. 61722507).

[1] K. K. Ni, S. Ospelkaus, M. H. G. de Miranda, A. Pe'er, B. Neyenhuis, J. J. Zirbel, S. Kotochigova, P. S. Julienne, D. S. Jin, and J. Ye, Science **322**, 231 (2008).

[2] W. Salzmann, U. Poschinger, R. Wester, M. Weidemuller, A. Merli, S. M. Weber, F. Sauer, M. Plewicki, F. Weise, A. M. Esparza, L. Woste, and A. Lindinger, Phys. Rev. A **73**, 023414 (2006).

[3] M. H. G. de Miranda, A. Chotia, B. Neyenhuis, D. Wang, G. Quemener, S. Ospelkaus, J. L. Bohn, J. Ye, and D. S. Jin, Nat. Phys. **7**, 502 (2011).

[4] T. Volz, N. Syassen, D. M. Bauer, E. Hansis, S. Duerr, and G. Rempe, Nat. Phys. **2**, 692 (2006).

[5] J. G. Danzl, E. Haller, M. Gustavsson, M. J. Mark, R. Hart, N. Bouloufa, O. Dulieu, H. Ritsch, and H.-C. Naegerl, Science **321**, 1062 (2008).

[6] T. M. Rvachov, H. Son, A. T. Sommer, S. Ebadi, J. J. Park, M. W. Zwierlein, W. Ketterle, and A. O. Jamison, Phys. Rev. Lett. **119**, 143001 (2017).

[7] B. Yan, S. A. Moses, B. Gadway, J. P. Covey, K. R. A. Hazzard, A. M. Rey, D. S. Jin, and J. Ye, Nature (London) **501**, 521 (2013).

[8] S. Jochim, M. Bartenstein, A. Altmeyer, G. Hendl, S. Riedl, C. Chin, J. Denschlag, and R. Grimm, Science **302**, 2101 (2003).

[9] H. Partridge, D. A. Dixon, S. P. Walch, C. W. Bauschlicher Jr., and J. L. Gole, J. Chem. Phys. **79**, 1859 (1983).

[10] B. Bussery and M. Aubert-Frécon, J. Chem. Phys. **82**, 3224 (1985).

[11] F. Spiegelmann, D. Pavolini, and J.-P. Daudey, J. Phys. B **22**, 2465 (1989).

[12] M. Krauss and W. J. Stevens, J. Chem. Phys. **93**, 4236 (1990).

[13] M. Foucrault, P. Millié, and J. P. Daudey, J. Chem. Phys. **96**, 1257 (1992).

[14] S. Kotochigova, E. Tiesinga, and P. S. Julienne, Phys. Rev. A: At. Mol. Opt. Phys. **63**, 012517 (2000).

[15] S. J. Park, S. W. Suh, Y. S. Lee, and G.-H. Jeung, J. Mol. Spectrosc. **207**, 129 (2001).

[16] A. A. Khuskivadze, M. I. Chibisov, and I. I. Fabrikant, Phys. Rev. A **66**, 042709 (2002).

[17] D. Edvardsson, S. Lunell, and C. M. Marian, Mol. Phys. **101**, 2381 (2003).

[18] M. Tomza, W. Skomorowski, M. Musiał, R. González-Férez, C. P. Koch, and R. Moszynski, Mol. Phys. **111**, 1781 (2013).

[19] W. Jastrzebski, P. Kowalczyk, J. Szczepkowski, A.-R. Allouche, P. Crozet, and A. J. Ross, J. Chem. Phys. **143**, 044308 (2015).

[20] C. Amiot and P. Crozet, Chem. Phys. Lett. **121**, 390 (1985).

[21] C. Amiot, J. Chem. Phys. **93**, 8591 (1990).

[22] J. Y. Seto, R. J. Le Roy, J. Vergès, and C. Amiot, J. Chem. Phys. **113**, 3067 (2000).

[23] B. Beser, V. B. Sovkov, J. Bai, E. H. Ahmed, C. C. Tsai, F. Xie, L. Li, V. S. Ivanov, and A. M. Lyyra, J. Chem. Phys. **131**, 094505 (2009).

[24] C. Amiot, O. Dulieu, and J. Vergès, Phys. Rev. Lett. **83**, 2316 (1999).

[25] H. Salami, T. Bergeman, B. Beser, J. Bai, E. H. Ahmed, S. Kotochigova, A. M. Lyyra, J. Huennekens, C. Lisdat, A. V. Stolyarov, O. Dulieu, P. Crozet, and A. J. Ross, Phys. Rev. A **80**, 022515 (2009).

[26] P. Kusch, Phys. Rev. **49**, 218 (1936).

[27] N. Tsi-Zé and T. San-Tsiang, Phys. Rev. **52**, 91 (1937).

[28] D. M. Creek and G. V. Marr, J. Quant. Spectrosc. Radiat. Transf. **8**, 1431 (1968).

[29] J. M. Brom Jr. and H. P. Broida, J. Chem. Phys. **61**, 982 (1974).

[30] D. L. Feldman and R. N. Zare, Chem. Phys. **15**, 415 (1976).

[31] D. L. Drummond and L. A. Schlie, J. Chem. Phys. **65**, 2116 (1976), erratum to [32].

[32] D. L. Drummond and L. A. Schlie, J. Chem. Phys. **66**, 1766 (1977), erratum to [31].

[33] R. Gupta, W. Happer, J. Wagner, and E. Wennmyr, J. Chem. Phys. **68**, 799 (1978).

[34] D. Kotnik-Karuza and C. R. Vidal, Chem. Phys. **40**, 25 (1979).

[35] C. D. Caldwell, F. Engelke, and H. Hage, Chem. Phys. **54**, 21 (1980).

[36] W.-T. Luh, J. T. Bahns, A. M. Lyyra, K. M. Sando, P. D. Kleiber, and W. C. Stwalley, J. Chem. Phys. **88**, 2235 (1988).

[37] F. Jenč and B. A. Brandt, Phys. Rev. A **39**, 4561 (1989).

[38] J. D. Miller, R. A. Cline, and D. J. Heinzen, Phys. Rev. Lett. **71**, 2204 (1993).

[39] R. A. Cline, J. D. Miller, and D. J. Heinzen, Phys. Rev. Lett. **73**, 632 (1994), errata to [40].

[40] R. A. Cline, J. D. Miller, and D. J. Heinzen, Phys. Rev. Lett. **73**, 2636 (1994), errata to [39].

[41] C. Amiot, Chem. Phys. Lett. **241**, 133 (1995).

[42] C. C. Tsai, R. S. Freeland, J. M. Vogels, H. M. J. M. Boesten, B. J. Verhaar, and D. J. Heinzen, Phys. Rev. Lett. **79**, 1245 (1997).

[43] C. Amiot and J. Vergès, Chem. Phys. Lett. **274**, 91 (1997).

[44] Y. Lee, Y. Yoon, S. J. Baek, D.-L. Joo, J.-s. Ryu, and B. Kim, J. Chem. Phys. **113**, 2116 (2000).

[45] Y. Yoon, Y. Lee, S. Lee, and B. Kim, J. Chem. Phys. **116**, 6660 (2002).

[46] R. F. Gutterres, C. Amiot, A. Fioretti, C. Gabbanini, M. Mazzoni, and O. Dulieu, Phys. Rev. A **66**, 024502 (2002).

[47] H. Jelassi, B. Viaris de Lesegno, and L. Pruvost, Phys. Rev. A **73**, 032501 (2006).

[48] T. Bergeman, J. Qi, D. Wang, Y. Huang, H. K. Pechkis, E. E. Eyler, P. L. Gould, W. C. Stwalley, R. A. Cline, J. D. Miller, and D. J. Heinzen, J. Phys. B **39**, S813 (2006).

[49] H. Jelassi, B. V. De Lesegno, and L. Pruvost, in *Fundamental and Applied Spectroscopy: Second International Spectroscopy Conference, ISC 2007*, edited by M. Telmini, N. T. Mliki, and E. Sediki, AIP Conf. Proc. No. 935 (AIP, New York, 2007), p. 203.

[50] Gabbanini, Nucl. Phys. A **790**, 757c (2007).

[51] R. Beuc, M. Movre, V. Horvatic, C. Vadla, O. Dulieu, and M. Aymar, Phys. Rev. A **75**, 032512 (2007).

[52] Y. Lee, S. Lee, and B. Kim, J. Phys. Chem. A **112**, 6893 (2008).

[53] J. Han and M. C. Heaven, J. Mol. Spectrosc. **268**, 37 (2011).

[54] T. Takekoshi, C. Strauss, F. Lang, J. H. Denschlag, M. Lysebo, and L. Veseth, Phys. Rev. A **83**, 062504 (2011).

[55] W. C. Stwalley, M. Bellos, R. Carollo, J. Banerjee, and M. Bermudez, Mol. Phys. **110**, 1739 (2012).

[56] X. Han, X. Wang, T. Wang, W. Xiong, and X. Dai, Chem. Phys. Lett. **538**, 1 (2012).

[57] Y. Guan, X. Han, J. Yang, Z. Zhou, X. Dai, E. H. Ahmed, A. M. Lyyra, S. Magnier, V. S. Ivanov, A. S. Skublov, and V. B. Sovkov, J. Chem. Phys. **139**, 144303 (2013).

[58] A. N. Drozdova, A. V. Stolyarov, M. Tamanis, R. Ferber, P. Crozet, and A. J. Ross, Phys. Rev. A **88**, 022504 (2013).

[59] H. Jelassi and L. Pruvost, Phys. Rev. A **89**, 032514 (2014).

[60] X. Han, J. Yang, Y. Guan, Z. Zhou, W. Zhao, A. R. Allouche, S. Magnier, E. H. Ahmed, A. M. Lyyra, and X. Dai, Chem. Phys. Lett. **601**, 124 (2014).

[61] M. Deiss, B. Drews, J. H. Denschlag, and E. Tiemann, New J. Phys. **17**, 083032 (2015).

[62] J. Yang, Z. Zhou, W. Zhao, X. Han, and X. Dai, J. Phys.: Conf. Ser. **635**, 032042 (2015).

[63] F. Bottcher, A. Gaj, K. M. Westphal, M. Schlagmueller, K. S. Kleinbach, R. Low, T. C. Liebisch, T. Pfau, and S. Hofferberth, Phys. Rev. A **93**, 032512 (2016).

[64] J. Yang, Y. Guan, W. Zhao, Z. Zhou, X. Han, J. Ma, V. B. Sovkov, V. S. Ivanov, E. H. Ahmed, A. M. Lyyra, and X. Dai, J. Chem. Phys. **144**, 024308 (2016).

[65] I. Havalyova, A. Pashov, P. Kowalczyk, J. Szczepkowski, and W. Jastrzebski, J. Quantum Spectrosc. Radiat. Transf. **202**, 328 (2017).

[66] A. Sanli, B. Beser, J. R. Edwardson, S. Magnier, E. H. Ahmed, and A. M. Lyyra, J. Chem. Phys. **143**, 104304 (2015).

[67] A. Fioretti, D. Comparat, A. Crubellier, O. Dulieu, F. Masnou-Seeuws, and P. Pillet, Phys. Rev. Lett. **80**, 4402 (1998).

[68] R. Carollo, M. A. Bellos, D. Rahmlow, J. Banerjee, E. E. Eyler, P. L. Gould, and W. C. Stwalley, Phys. Rev. A **87**, 022505 (2013).

[69] A. Altaf, S. Dutta, J. Lorenz, J. Perez-Rios, Y. P. Chen, and D. S. Elliott, J. Chem. Phys. **142**, 114310 (2015).

[70] D. Wang, E. E. Eyler, P. L. Gould, and W. C. Stwalley, Phys. Rev. A **72**, 032502 (2005).

[71] Y. Huang, J. Qi, H. K. Pechkis, D. Wang, E. E. Eyler, P. L. Gould, and W. C. Stwalley, J. Phys. B At. Mol. Opt. Phys. **39**, S857 (2006).

[72] S. Sainis, J. Sage, E. Tiesinga, S. Kotochigova, T. Bergeman, and D. DeMille, Phys. Rev. A **86**, 022513 (2012).

[73] A. Haerter, A. Kruekow, M. Deiss, B. Drews, E. Tiemann, and J. H. Denschlag, Nat. Phys. **9**, 512 (2013).

[74] A. Kirrander, S. Rittenhouse, M. Ascoli, E. E. Eyler, P. L. Gould, and H. R. Sadeghpour, Phys. Rev. A **87**, 031402(R) (2013).
[75] E. Reinhold and W. Ubachs, Mol. Phys. **103**, 1329 (2005).
[76] S. Mollet and F. Merkt, Phys. Rev. A **82**, 032510 (2010).
[77] M. Beyer and F. Merkt, J. Chem. Phys. **149**, 031102 (2018).
[78] R. J. Le Roy, Y. Huang, and C. Jary, J. Chem. Phys. **125**, 164310 (2006).
[79] R. J. Le Roy and R. D. E. Henderson, Mol. Phys. **105**, 663 (2007).
[80] J. A. Coxon and P. G. Hajigeorgiou, J. Chem. Phys. **132**, 094105 (2010).
[81] V. B. Sovkov, V. S. Ivanov, K. V. Minaev, and M. S. Aleksandrov, Opt. Spectrosc. **114**, 167 (2013).
[82] C. Strauss, T. Takekoshi, F. Lang, K. Winkler, R. Grimm, J. Hecker Denschlag, and E. Tiemann, Phys. Rev. A **82**, 052514 (2010).
[83] P. T. Arndt, V. B. Sovkov, J. Ma, X. Pan, D. S. Beecher, J. Y. Tsai, Y. Guan, A. M. Lyyra, and E. H. Ahmed, J. Chem. Phys. **149**, 224303 (2018).
[84] B. A. Palmer, R. A. Keller, and R. Engleman Jr., *An Atlas of Uranium Emission Intensities in a Hollow Cathode Discharge*, Technical Report No. LA-8251-MS (Los Alamos Scientific Laboratory, New Mexico, 1980).
[85] See Supplemental Material at http://link.aps.org/supplemental/10.1103/PhysRevA.99.052511 for the experimental term values, semiempirical tabulated model, and RKR potential functions of the Rb_2 $6^1\Sigma_g^+$ state.
[86] V. B. Sovkov, F. Xie, A. M. Lyyra, E. H. Ahmed, J. Ma, and S. Jia, J. Chem. Phys. **147**, 104301 (2017).
[87] J. O. Hirschfelder, C. F. Curtiss, and R. B. Bird, *Molecular Theory of Gases and Liquids* (Wiley, New York, 1966).
[88] M. Marinescu and A. Dalgarno, Phys. Rev. A **52**, 311 (1995).
[89] M. Marinescu and A. Dalgarno, Z. Phys. D **36**, 239 (1996).
[90] A. A. Šurkus, R. J. Rakauskas, and A. B. Bolotin, Chem. Phys. Lett. **105**, 291 (1984).
[91] E. V. Shikin and A. I. Plis, *Handbook on Splines for the User* (CRC, Boca Raton, FL, 1995).
[92] J. M. Blatt, J. Comput. Phys. **1**, 382 (1967).
[93] R. J. Le Roy, J. Quantum Spectrosc. Radiat. Transf. **186**, 167 (2017).
[94] V. B. Sovkov and J. Ma, in *Proceedings of the 2016 International Conference on Applied Mathematics, Simulation and Modelling*, Advances in Computer Science Research, edited by A. Dadvand, K. Nagaraja, and M. Mirzazadeh (Atlantis Press, Beijing, China, 2016), Vol. 083, pp. 369–372.
[95] D. W. Marquardt, J. Soc. Industr. Appl. Math. **11**, 431 (1963).
[96] G. H. Golub and C. F. Loan, *Matrix Computations*, 3rd ed. (The John Hopkins University Press, Baltimore, 1996).
[97] R. Rydberg, Z. Phys. **73**, 376 (1932).
[98] R. Rydberg, Z. Phys. **80**, 514 (1933).
[99] O. Klein, Z. Phys. **76**, 226 (1932).
[100] A. L. G. Rees, Proc. Phys. Soc. London **59**, 998 (1947).
[101] R. J. Le Roy, J. Mol. Spectrosc. **191**, 223 (1998).
[102] T. Ban, R. Beuc, H. Skenderovic, and G. Pichler, Europhys. Lett. **66**, 485 (2004).
[103] J. P. Shaffer, S. T. Rittenhouse, and H. R. Sadeghpour, Nat. Commun. **9**, 1965 (2018).